NASA TECHNICAL MEMORANDUM

NASA TM X- 72001

COPY NO.

NASA TM X- 72001

HEATING ANALYSIS FOR THE PIONEER VENUS

MULTIPROBE MISSION

By

Kenneth Sutton

July 1974

This informal documentation medium is used to provide accelerated or special release of technical information to selected users. The contents may not meet NASA formal 'iting and publication standards, may be revised, or may be incorporated in another publication.

NATIONAL AERONAUTICS AND SPACE ADMINISTRATION

LANGLEY RESEARCH CENTER, HAMPTON, VIRGINIA 23665

1. Report No. NASA TM X-72001	2. Government Accession No.	3. Recipient's Catalog No.
4. Title and Subtitle HEATING ANALYSIS FOR THE PIONEER VENUS MULTIPROBE MISSION		5. Report Date July 1974
		6. Performing Organization Code
7. Author(s) Kenneth Sutton		8. Performing Organization Report No.
		10. Work Unit No.
9. Performing Organization Name and Address Gas Radiation Section/AEAB/SSD NASA-Langley Research Center Hampton, VA 23665		11. Contract or Grant No.
		13. Type of Report and Period Covered High-Number TM X
12. Sponsoring Agency Name and Address NASA-Langley Research Center Hampton, VA 23665		14. Sponsoring Agency Code 506-26-20-06

15. Supplementary Notes

16. Abstract

Results are presented for the fully-coupled, radiating flow field around the entry probes from a detailed calculation which includes equilibrium chemistry, nongray radiative transport, ablation product injection, and a laminar or turbulent boundary layer. These results show that the radiative flux toward the body is attenuated in the boundary layer at downstream regions of the body as well as at the stagnation point and that, even when radiation absorption by ablation products is accounted for, the radiative heating rates along the downstream regions of the body can, under certain conditions, exceed the stagnation-point values. It is also shown that, for Venusian entry, the spectral distribution of radiative flux and the magnitude of radiation absorption by ablation products depend strongly on entry velocity, and that the state of the boundary layer (i.e., laminar or turbulent) can significantly influence the amount of ablation product absorption or emission that occurs in various spectral regions. Results from a series of radiative, inviscid calculations are also presented.

17. Key Words (Suggested by Author(s)) (STAR category underlined) Venusian Entry, Radiative Heating, Thermodynamics & Combustion, Fluid Mechanics, Space Vehicles	18. Distribution Statement		
19. Security Classif. (of this report) Unclassified	20. Security Classif. (of this page) Unclassified	21. No. of Pages 30	22. Price* $3.25

ABSTRACT

Results are presented for the fully-coupled, radiating flow
field around the entry probes from a detailed calculation which includes
equilibrium chemistry, nongray radiative transport, ablation product
injection, and a laminar or turbulent bou.dary layer. These results
show that the radiative flux toward the body is attenuated in the
boundary layer at downstream regions of the body as well as at the
stagnation point and that, even when radiation absorption by ablation
products is accounted for, the radiative heating rates along the down-
stream regions of the body can, under certain conditions, exceed
the stagnation-point values. It is also shown that, for Venusian
entry, the spectral distribution of radiative flux and the magnitude
of radiation absorption by ablation products depend strongly on
entry velocity, and that the state of the boundary layer (i.e., laminar
or turbulent) can significantly influence the amount of ablation pro-
duct absorption or emission that occurs in various spectral regions.
Results from a series of radiative, inviscid calculations are also
presented.

INTRODUCTION

The proposed multi-probe mission to Venus, Pioneer Venus, is the first for which radiative heating is a dominant feature of the aero-thermodynamic environment and for which a detailed analysis of radiative heating is needed to evaluate heatshield requirements. The Advanced Entry Analysis Branch at the Langley Research Center has a continuing program for the development of analytical techniques for calculation of the radiating flow field about planetary entry bodies. A recently developed technique has been used to obtain several benchmark solutions, which are presented herein, for conditions near peak heating for the Pioneer Venus probes.

This technique provides for the calculation of the fully-coupled, viscous, radiating flow field about an ablating axisymmetric body. Detailed treatments of nongray radiative transport; equilibrium chemistry; and mass, momentum and energy transport are included. The flow may be either laminar or turbulent and the ablation rate is determined as part of the solution through a steady-state ablation calculation.

Results from a series of inviscid calculations are also presented. These inviscid solutions were obtained in order to determine the radiative heating history during entry of the probes, the effect of the composition of the Venusian atmosphere on radiative heating, and to explore the effect of certain changes in probe geometry on radiative heating.

SYMBOLS

h_∞	freestream enthalpy
m_a	ablation rate of the heat shield
P_∞	freestream pressure
q^C	convective heating rate
q^R	radiative heating rate
R_{e_θ}	momentum thickness Reynolds number for boundary layer
R_n	nose radius of body
R_b	base radius of body
s	distance along body surface
t	trajectory time
T	temperature
V_e	entry velocity
V_∞	freestream velocity
W	weight of entry probe
$W/C_d A$	ballistic coefficient
γ_e	entry angle
θ_c	cone angle of body
ρ_∞	freestream density
τ	aerodynamic shear

Subscripts:

e	refers to the boundary-layer edge
w	refers to the body wall
o	refers to the stagnation point
ν	refers to radiation frequency

METHOD OF SOLUTION

A complete description of the method for the fully coupled solution of the radiative flow field around an ablating entry body is given in references 1 and 2. Briefly, the method of solution is to separate the flow field into an outer layer where the inviscid flow equations are applicable and an inner viscous layer, either laminar or turbulent, where the boundary layer equations are applicable. The divergence of the radiative flux is included in the energy equation for the solution of each layer and the boundary layer is coupled to the inviscid shock layer by the radiative transport through both layers and by the boundary layer displacement thickness. In the coupling of the two layers, the inviscid flow field is displaced from the wall by the boundary layer displacement thickness and the boundary layer profiles are used out to the point where the boundary layer edge properties and their derivatives equal the corresponding inviscid layer values. The radiative transport for the boundary layer solution is calculated from the matched profiles through the entire layer. The treatment of radiation includes molecular band, continuum, and line transitions with a detailed frequency dependence of the absorption coefficient. The ablation rate is computed as part of the solution under the assumption of steady-state ablation.

Several solution options are available. One is the fully-coupled solution described previously. A second is an inviscid full flow-field solution; and the third an inviscid stagnation-region solution.

RESULTS AND DISCUSSIONS

Fully-coupled solutions at typical conditions were obtained for the entry probes of Pioneer Venus. The entry trajectories used in the analysis are presented in Figure 1 and were calculated from nominal entry parameters and body shapes provided by the Pioneer Venus Study Team of the Ames Research Center. The atmospheric model for the Venusian atmosphere is that presented in reference 3 with the gas composition 97 percent carbon dioxide and 3 percent nitrogen by volume.

The radiative heating rates at the stagnation point of the bodies were calculated along the trajectories to determine the location of peak radiative heating. The "stagnation-point" version of the radiating inviscid flow program was used for these calculations. The results are presented in Figure 2 for the large and small probes. Even though the nose radius is smaller, the radiative heating to the small probe is greater due to its deeper penetration into the denser regions of the atmosphere at high velocities. Also, two peaks occur in the radiative heating to the small probe. At the higher velocities, the thermodynamic state of the gas behind the shock is such that line radiation is a large contributor of the total radiative heating; however, the contribution of line radiation decreases as the entry probe decelerates and molecular band radiation becomes important. The large probe decelerates at a higher altitude and the radiative

heating to the probe is almost constant during the time of maximum radiative heating. The possibility of a double peak in the time history of radiative heating to a probe will depend on the entry trajectory.

The flight conditions represented by circular symbols in Figure 2 were chosen as being representative of peak heating. It is at these conditions for peak radiative heating that fully coupled solutions with ablation product effects were obtained for the flow around the large and small probes. Hereafter, these are referred to as large and small probe solutions. The ablation of the heat shield for the fully coupled solution is represented by steady-state ablation of a phenolic carbon material with elemental mass fractions of carbon, 0.851; oxygen, 0.110; hydrogen, 0.035; and nitrogen, 0.004. The steady-state ablation rates are obtained as part of the fully coupled solution and are not prespecified.

The results from the fully coupled solutions for the large and small probes are presented in Figures 3 and 4, respectively. The distribution along the body of radiative heating, convective heating, ablation rate, aerodynamic shear, and momentum thickness Reynolds number are presented. The spectral distribution of radiative heat flux due to continuum processes is also presented for two body locations. At these flight conditions, the line radiation is small compared to the continuum.

For the large probe, the ablation rate decreases in the nose region and reaches a nearly constant value along the afterbody (Fig. 3(d)). As shown in Figure 3(c), the convective heating rate decreases along the afterbody but the radiative heating rate increases to values which exceed the stagnation-point value. The radiative heating to the wall is greater than the convective heating along the entire body. The total heating rate, radiative plus convective, along the afterbody is 30 percent to 40 percent less than the stagnation-point value. Thus, the decrease in convective heating rate along the afterbody counterbalances the effect of the increase in radiative heating rate. The wall temperature resulting from the steady-state ablation is 3600° K, within 2 percent, along the entire body.

For the small probe, there is a decrease in the ablation rate along the afterbody (Fig. 4(d)) and both the convective and radiative heating rates decrease along the afterbody (Fig. 4(c)). The convective heating rate is greater than the radiative heating rate along the entire body. This result is opposite to the result obtained for the large probe. The total heating rate along the afterbody of the small probe is 40 percent to 60 percent less than the stagnation point value. The wall temperature resulting from the steady-state ablation is 3700° K, within 2 percent along the body.

The radiative heating rates from inviscid, radiating solutions are compared with the results for the fully coupled solutions with

steady-state ablation in Figures 3(b) and 4(b) for the large and small probes, respectively. The radiative heating rates from the fully coupled solutions are less than the values from the inviscid, radiating solutions by 9 percent and 17 percent, respectively, for the large and small probes at the stagnation point of the bodies. These percent reductions are nearly constant along the bodies. The reduction in radiative heating is due to absorption of radiation within the boundary layer.

Spectral distributions of radiative heating toward the body due to continuum processes are presented in Figures 3(g) and 4(g), respectively, for the large and small probes. (Note, molecular band radiation is included with the continuum radiation and both are referred to as continuum processes). The spectral distributions are presented for the stagnation point and an afterbody location. As shown by the results, the absorption of radiation within the boundary layer occurs in the spectral range of 5 to 10 eV and is due to self-absorption of the fourth positive band system of carbon monoxide, $CO(4+)$. At the stagnation point of the small probe there is a slight increase in radiative heating within the boundary layer at 2.5 eV that is due to the Swan band system of diatomic carbon, $C_2(S)$. A similar effect was noted at the other body locations for both the large and small probes, but the effect was too small to be presented in the figures. The radiative heating due to line processes was less than 10 percent of the total radiative heating at these entry conditions and spectral distributions are not presented.

The fully coupled solutions assumed laminar flow in the boundary layer. Shown in Figures 3(f) and 4(f) are the distributions of momentum thickness Reynolds number around the bodies. If the critical value for transition to turbulent flow is about 200, then the boundary layer would be turbulent along the afterbody for both the large and small probes. This could have an appreciable effect on the distribution of convective heating, ablation rate, and aerodynamic shear.

A fully coupled solution for the large probe with a turbulent boundary layer was obtained and the results are compared with the laminar case in Figure 5. A critical value of 200 for the momentum thickness Reynolds number was used for instantaneous transition to turbulent flow. As expected, the convective heating rates, ablation rates, and aerodynamic shears increased with transition to turbulent flow. The distribution of radiative heating along the body was essentially the same for both laminar and turbulent flow; thus, the turbulent boundary layer did not appear to further attenuate the radiative heating even though the boundary-layer thickness was as much as 80 percent greater than for laminar flow. This phenomenon can be explained with the spectral distributions of radiative flux at the wall presented in Figure 5(d) for the turbulent and laminar solutions. For the turbulent boundary layer, there is an increase in the self-absorption of the $CO(4+)$ band system in the spectral range of 5 to 8 eV but this effect is offset by an increased emission of the $C_2(S)$

band system at 2.5 eV and the red band system of cyanogen, CN(R),
at 0.6 to 2 eV. The spectral distribution at the boundary-layer
edge is essentially the same for both the turbulent and laminar boundary
layers and was presented in Figure 3(g). While the radiative heating
rates along the afterbody of the large probe are the same for a tur-
bulent or a laminar boundary layer, the wall spectral distribution
of the radiation is different for the two cases. It should not be
inferred that the radiative heating to the body will be the same for
a laminar or turbulent boundary layer for other entry conditions or
other body shapes.

A fully coupled solution was obtained for freestream conditions
representative of a higher entry velocity than that of the nominal
trajectories,and the results are presented in Figure 6. The freestream
conditions and body shape are given in Figure 6(a). The body shape
is the same as the large probe except the nose radius is slightly
smaller. Hereafter, this case is referred to as the high velocity
entry.

As shown in Figure 6(c), the radiative heating rate is greater
than the convective heating rate along the entire body. Unlike the
results previously presented for the large probe, there is only a
slight increase in the radiative heating along the afterbody. The
convective heating rate at the stagnation point is slightly less
than the values just downstream of the stagnation point due
to an increased effect of blockage of convective heating by the mass

injection of the ablation products. As shown in Figure 9(d), the ablation rate decreases along the body in the nose region. The ablation rate and total heating rate are nearly constant along the afterbody. The wall temperature resulting from the steady-state ablation is 3750° K, within 1 percent, along the body.

There is significant absorption of radiation within the boundary layer for the high velocity entry as shown by comparison of results between the fully coupled solution and an inviscid, radiating solution in Figure 6(b). The reduction in radiative heating rate is 25 percent at the stagnation point and 25 percent to 30 percent along the afterbody. Spectral distributions of radiative heating toward the body due to continuum processes are presented in Figure 6(g) for the stagnation point and an afterbody location. For the continuum processes, most of the absorption within the boundary layer occurs in the spectral region of 5 to 10 eV and is due mainly to self-absorption of the CO(4+) band. There is an increase in radiative flux at 2.5 eV and is due to the $C_2(S)$ band. At the stagnation point there is absorption at photon energies greater than 10 eV and this absorption is attributed to atomic species within the cooler regions of the boundary layer. There is also absorption at the photoionization edge of carbon at 8.5 eV.

The radiative flux due to line processes is 50 percent of the total radiative flux at the nose region of the body and decreases to only 20 percent along the afterbody. Spectral distributions of the

radiative heating due to line processes for two locations at the nose region are presented in Figure 6(h). Absorption of line radiation within the boundary layer occurs only for the line groups in the ultra-violet at 7.1, 8.4, and 9.4 eV. The line radiation in the visible and infrared regions of the spectrum, less than 2 eV, is not attenuated within the boundary layer.

Information on the effects of different heatshield materials on the attenuation of radiative heating within the boundary layer would be useful in the final design of the entry probes. The only heat-shield material considered in the present study was phenolic carbon; thus, the effect of the heatshield material on the results cannot be determined directly. However, the results at the stagnation point for the high velocity case can be compared with prior results pre-sented in reference 4 for a phenolic nylon material (elemental mass fractions of carbon, 0.61; oxygen, 0.20; hydrogen, 0.10; and nitrogen, 0.09). The freestream conditions and body nose radius were the same as the present high velocity solution except the freestream gas com-position was 90 percent CO_2, 10 percent N_2 for the solution of ref-erence 4. A tabulation of the results is presented below.

Material	Present Phenolic Carbon	Reference 4 Phenolic Nylon
q_w^R, MW/m^2	26.7	20.8
q_e^R, MW/m^2	36.3	30.7
q_w^C, MW/m^2	3.2	2.9
m_a, kg/m^2-s	0.98	0.84
T_w, $^\circ$K	3770.0	3440.0

The results from the two solutions are in general agreement with the ablation rate, convective heating rate, and radiative heating rate being slightly lower for the phenolic nylon material. The attenuation of radiative heating within the boundary layer $(q_e^R - q_w^R)$ was 10 MW/m^2 for both materials. A strong conclusion cannot be made about the effect of the heatshield material due to slight differences in computational procedure and freestream gas composition for the two solutions. The phenolic nylon material appears to be slightly better from the standpoint of lower heating rates and ablation rate at this entry condition. However, the phenolic nylon may be more susceptable to char failure.

The exact composition of the Venusian atmosphere is unknown at present. The most recent data indicates the composition to be predominately CO_2 (up to 100 percent) with the other principal constituent being N_2. The effect of gas composition for CO_2-N_2 mixtures on the inviscid, radiative heating to the stagnation point of a body is presented in Figure 7 for two entry conditions. For the higher velocity entry, the radiative heating rate varies by only 25 percent over the range of CO_2 content with the higher values occurring for the greater percentage of CO_2. For the lower velocity entry, the radiative heating rate can vary by a factor of 6 over the range of CO_2 content. This is due to the domination of radiation by the molecular band transitions of $CO(4+)$, $CN(V)$, and $CN(R)$ at the lower velocity. For the compositions of present interest for Venusian entry (less than 10 percent N_2), the effect of composition on the stagnation-point, radiative heating rate is negligible at the higher velocity; but, a 22 percent difference occurs with composition at the lower velocity.

During the evolution of the Pioneer Venus project, two differ-
ent sets of entry probes have been studied. The first probe set,
referred to hereafter as Type I probes, consisted of a large probe
which had a 60° cone angle and three small probes which had 45° cone
angles. The second set of probes, referred to hereafter as Type II
probes, consisted of a large probe and three small probes, all of
which had 45° cone angles. In addition to the differences in cone
angle, there were also differences in nose radii and ballistic coef-
ficients between the two probe sets. The characteristics of the Type
I and Type II probes and their respective entry trajectories are
presented in figure 8. The only small probe considered for each
probe set is the one entering at the steepest entry angle.

The time histories of cold-wall, convective heating rate and
inviscid, radiative heating for the stagnation point of the probes
are presented in Figure 9. The cold-wall, convective heating rates
were calculated by

$$q^c_{w,o} \sqrt{R_n} = 1.88 \times 10^{-4} \rho_\infty^{1/2} V_\infty^3$$

and this equation is based on the method presented in reference 5 for
the heat transfer coefficient. Both the radiative and convective
heating rates for the large probe are greater for Type II than Type I
and are due to the deeper penetration into the denser regions of
the atmosphere at high velocities. For the small probe, the main
difference is a decrease in convective heating for Type II and is
due to increased nose radius.

The inviscid, radiative heating distributions along the body at times near peak heating are presented in Figure 10 for the two probe sets. A substantial change in the distribution for the large probe resulted from a decrease in conical angle from 60 to 45 degrees. The radiative heating rate increases along the conical region for the 60° body but decreases along the conical region for the 45° body. While the stagnation point value for the large probe is 60 percent greater for Type II than Type I, the values along the flank region (where the heatshield area is largest) decreased by 50 percent.

CONCLUSIONS

A computational method developed for the solution of the radiating flow field around planetary entry bodies has been used to obtain results for the entry probes of the proposed Pioneer Venus mission.

The method is a detailed calculation for a fully-coupled radiating flow field with ablation product injection into a laminar or turbulent boundary layer. The results from the present study for the entry probes of Pioneer Venus show that the radiative flux toward the body is attenuated in the boundary layer at downstream regions of the body as well as at the stagnation point, and that, even when radiation absorption by ablation products is accounted for, the radiative heating rates along the downstream regions of the body can, under certain conditions, exceed the stagnation-point values. It is also shown that, for Venusian entry, the spectral distribution of radiative flux and the magnitude of radiation absorption by ablation products depend strongly on entry velocity, and that the state of the boundary layer (i.e., laminar or turbulent) can significantly influence the amount of ablation product absorption or emission that occurs in various spectral regions.

The attenuation of radiation by the boundary layer will reduce the radiative heating to the body by up to 20 percent for the entry conditions and body shapes which are presently considered as nominal for Pioneer Venus. The reduction increases to 30 percent at higher velocity entries.

REFERENCES

1. Sutton, Kenneth: Characteristics of Coupled Nongray Radiating Gas Flows with Ablation Product Effects about Blunt Bodies During Planetary Entries. Ph.D. Thesis, Department of Mechanical and Aerospace Engineering, North Carolina State University at Raleigh, 1973.

2. Sutton, Kenneth: Fully Coupled Nongray Radiating Gas Flows with Ablation Product Effects about Planetary Entry Bodies. AIAA Paper No. 73-672, 1973.

3. Ames Research Center. "Pioneer Venus." Report of a Study by the Science Steering Group. Ames Research Center, Moffett Field, California, 1972.

4. Sutton, Kenneth and Falanga, R. A.: Stagnation Region Radiative Heating with Steady-State Ablation during Venus Entry. AIAA J., Vol. 10, No. 2, pp. 155-157. Feb. 1973.

5. Sutton, Kenneth and Graves, Randolph A., Jr.: A General Stagnation-Point Convective-Heating Equation for Arbitrary Gas Mixtures. NASA TR R-376, 1971.

Figure 2. STAGNATION-POINT SOLUTION
O AROUND BODY SOLUTION

SMALL PROBE

LARGE PROBE

$q_{w,0}^R$, MW/m^2

V_∞, km/s

Figure 2.- Stagnation-point, radiative heating rates along entry trajectories for large and small probes. Results from radiating, inviscid flow solutions.

	LARGE PROBE	SMALL PROBE
V_e =	11.06 km/s	11.06 km/s
γ_e =	-42^0	-56^0
$W/C_d A$ =	78.5 kg/m^2	125.7 kg/m^2
W =	158.3 kg	22.7 kg

LARGE PROBE

SMALL PROBE

ALTITUDE, km

VELOCITY, km/s

Figure 1.- Trajectories for large and small probes during entry to Venus.

GAS COMPOSITION BY VOLUME
.97 CO_2 - .03 N_2

$V_\infty = 8.803$ km/s

$\rho_\infty = 5.79 \times 10^{-3}$ kg/m^3

$p_\infty = 200.1$ N/m^2

$h_\infty = -8.86$ MJ/kg

$R_n = 0.3429$ m

$\theta_c = 60^0$

(a) FREE-STREAM CONDITIONS AND BODY SHAPE

(b) COMPARISON OF RADIATIVE HEATING

INVISCID, RADIATING SOLUTION

FULLY-COUPLED SOLUTION

q_w^R, MW/m^2

s/Rn

(c) RADIATIVE AND CONVECTIVE HEATING DISTRIBUTION

RADIATIVE HEATING

CONVECTIVE HEATING

q_w, MW/m^2

(d) ABLATION RATE DISTRIBUTION

m_a, kg/m^2-s

s/Rn

(e) AERODYNAMIC SHEAR DISTRIBUTION

τ_w, kN/m^2

(f) MOMENTUM THICKNESS REYNOLDS NUMBER DISTRIBUTION

Re_θ

s/Rn

(g) SPECTRAL DISTRIBUTION OF RADIATIVE HEATING TOWARD THE BODY DUE TO CONTINUUM PROCESSES

s/Rn = 2.0

BOUNDARY-LAYER EDGE

WALL

$q_\nu^{R,-}$, MW m^2-eV

s/Rn = 0

BOUNDARY-LAYER EDGE

WALL

$q_\nu^{R,-}$, MW m^2-eV

PHOTON ENERGY, eV
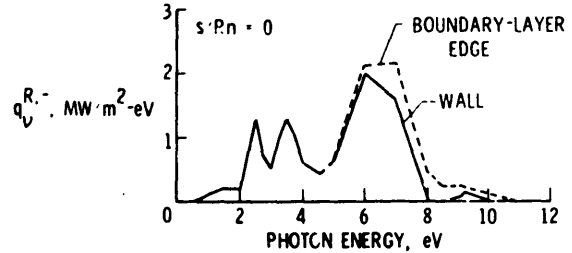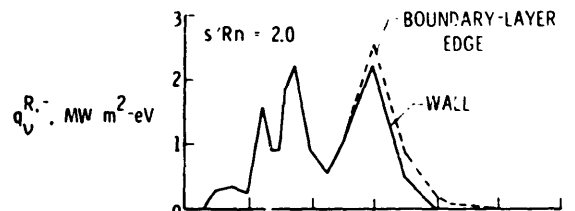
Figure 3.- Fully coupled, radiating flow solution with steady-state ablation of carbon-phenolic heat shield for large probe.

GAS COMPOSITION BY VOLUME
.97 CO_2 - .03 N_2

V_∞ = 9.331 km/s
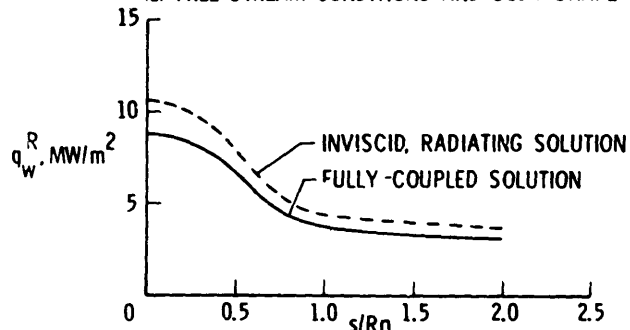
ρ_∞ = 9.32 × 10^{-3} kg/m^3

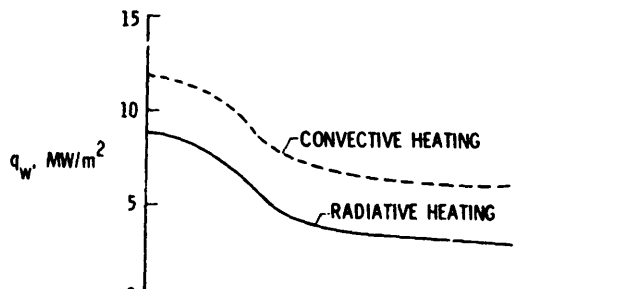p_∞ = 330.4 N/m^2

h_∞ = -8.86 MJ/kg

Rn = 0.1397 m

ϑ_c = 45^0

(a) FREE-STREAM CONDITIONS AND BODY SHAPE

(b) COMPARISON OF RADIATIVE HEATING

INVISCID, RADIATING SOLUTION

FULLY-COUPLED SOLUTION

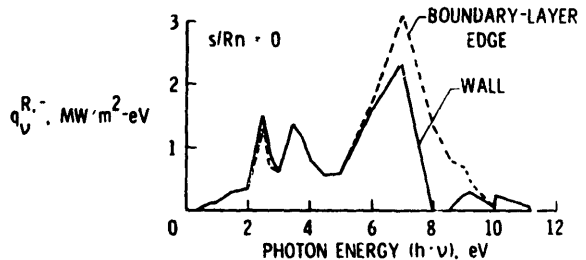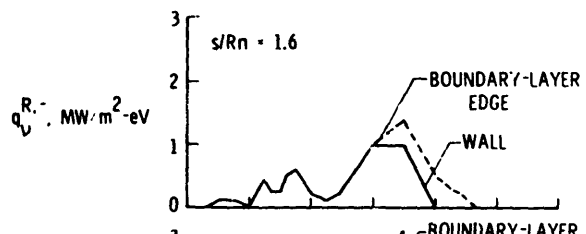(c) RADIATIVE AND CONVECTIVE HEATING DISTRIBUTION

CONVECTIVE HEATING

RADIATIVE HEATING

(d) ABLATION RATE DISTRIBUTION

(e) AERODYNAMIC SHEAR DISTRIBUTION

(f) MOMENTUM THICKNESS REYNOLDS NUMBER DISTRIBUTION

s/Rn = 1.6

BOUNDARY-LAYER EDGE

WALL

s/Rn = 0

BOUNDARY-LAYER EDGE

WALL

(g) SPECTRAL DISTRIBUTION OF RADIATIVE HEATING TOWARD THE BODY DUE TO CONTINUUM PROCESSES

Figure 4.- Fully coupled, radiating flow solution with
steady-state ablation of carbon-phenolic
heat shield for small probe.

(a) HEATING RATE DISTRIBUTION

(b) ABLATION RATE DISTRIBUTION

(c) AERODYNAMIC SHEAR DISTRIBUTION

(d) SPECTRAL DISTRIBUTION AT THE WALL OF RADIATIVE HEATING TOWARD THE BODY DUE TO CONTINUUM PROCESSES
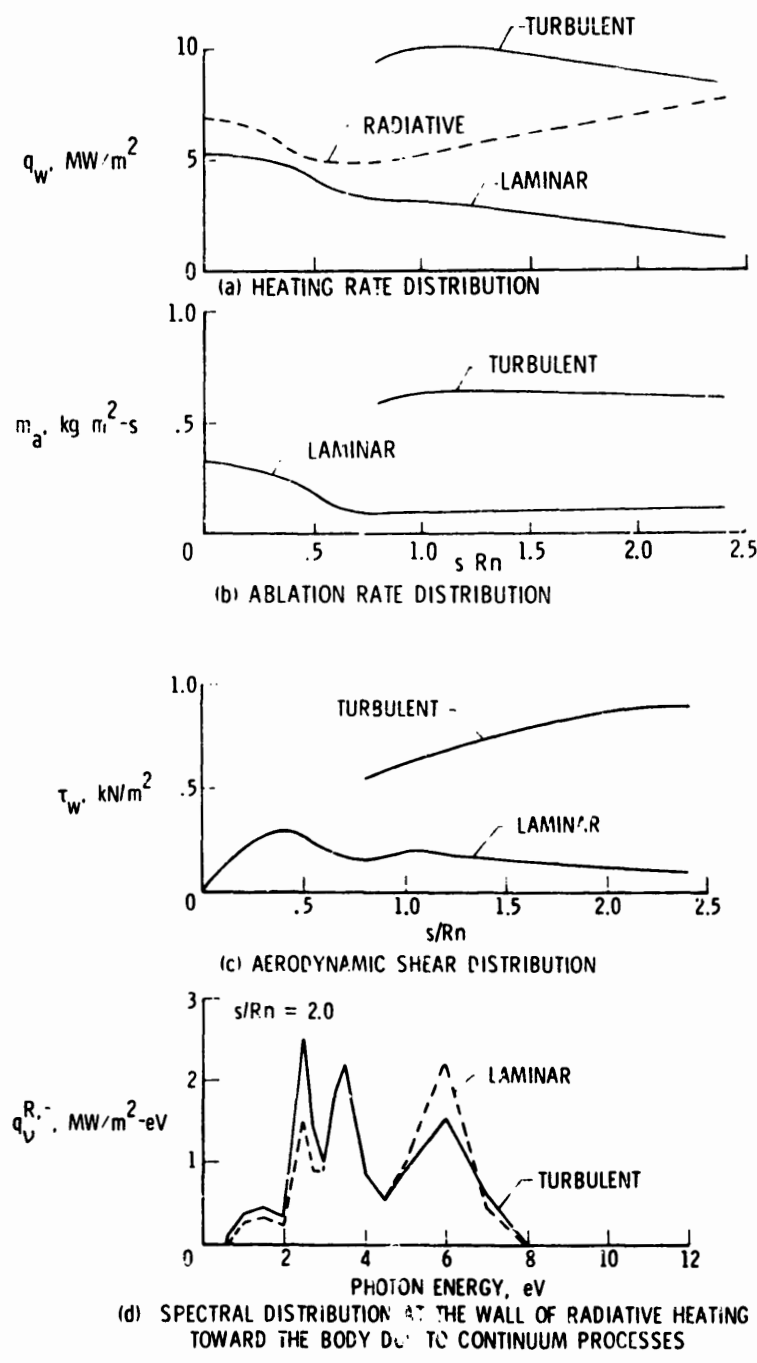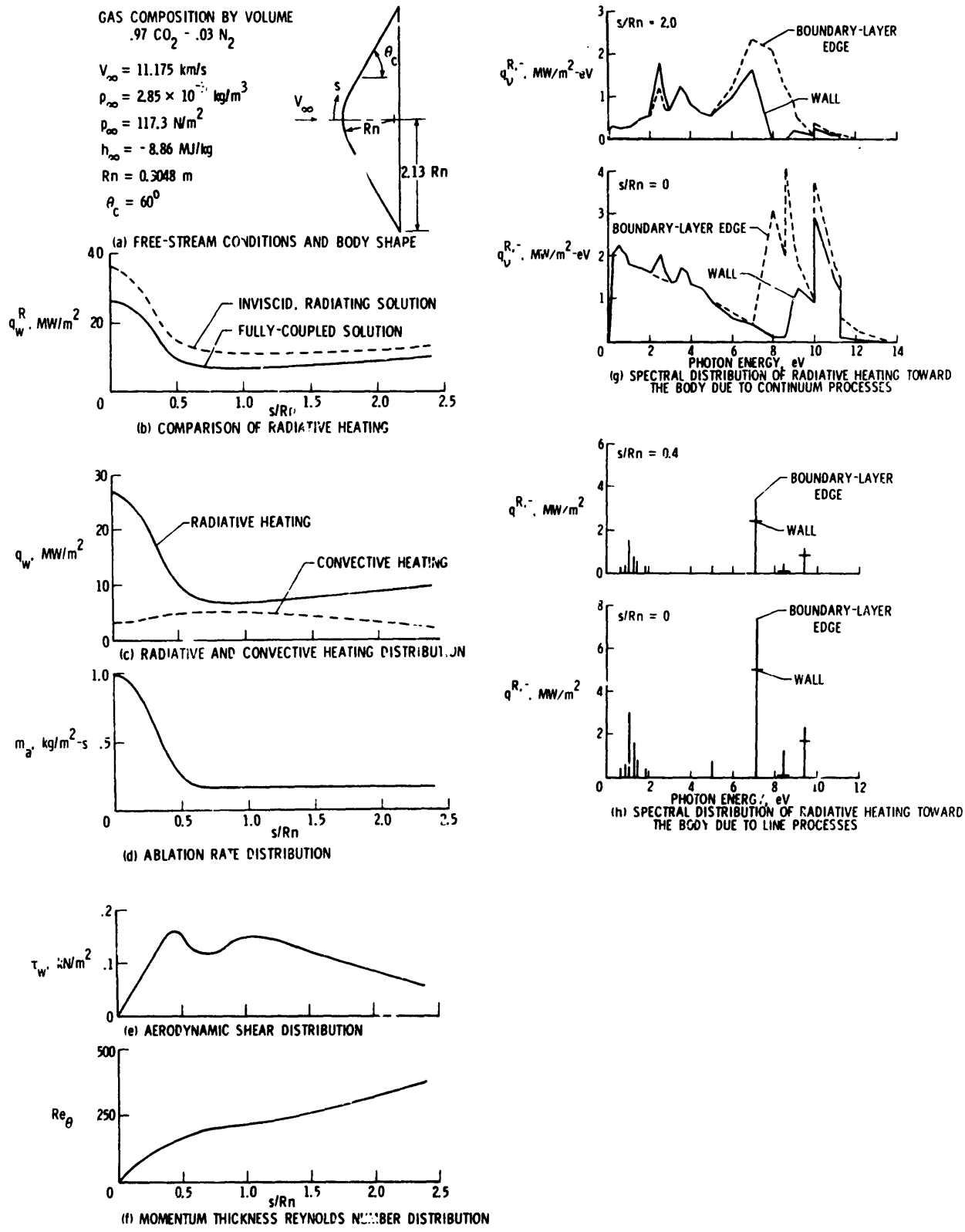
Figure 5.- Comparison between a turbulent and laminar boundary layer for fully coupled solution for large probe.

(a) FREE-STREAM CONDITIONS AND BODY SHAPE

GAS COMPOSITION BY VOLUME
.97 CO_2 - .03 N_2

V_∞ = 11.175 km/s

ρ_∞ = 2.85 × 10$^{-?}$ kg/m^3

p_∞ = 117.3 N/m^2

h_∞ = - 8.86 MJ/kg

Rn = 0.3048 m

θ_c = 60°

(b) COMPARISON OF RADIATIVE HEATING

INVISCID, RADIATING SOLUTION
FULLY-COUPLED SOLUTION

(c) RADIATIVE AND CONVECTIVE HEATING DISTRIBUTION

RADIATIVE HEATING
CONVECTIVE HEATING

(d) ABLATION RATE DISTRIBUTION

(e) AERODYNAMIC SHEAR DISTRIBUTION

(f) MOMENTUM THICKNESS REYNOLDS NUMBER DISTRIBUTION

(g) SPECTRAL DISTRIBUTION OF RADIATIVE HEATING TOWARD THE BODY DUE TO CONTINUUM PROCESSES

s/Rn = 2.0
BOUNDARY-LAYER EDGE
WALL

s/Rn = 0
BOUNDARY-LAYER EDGE
WALL

(h) SPECTRAL DISTRIBUTION OF RADIATIVE HEATING TOWARD THE BODY DUE TO LINE PROCESSES

s/Rn = 0.4
BOUNDARY-LAYER EDGE
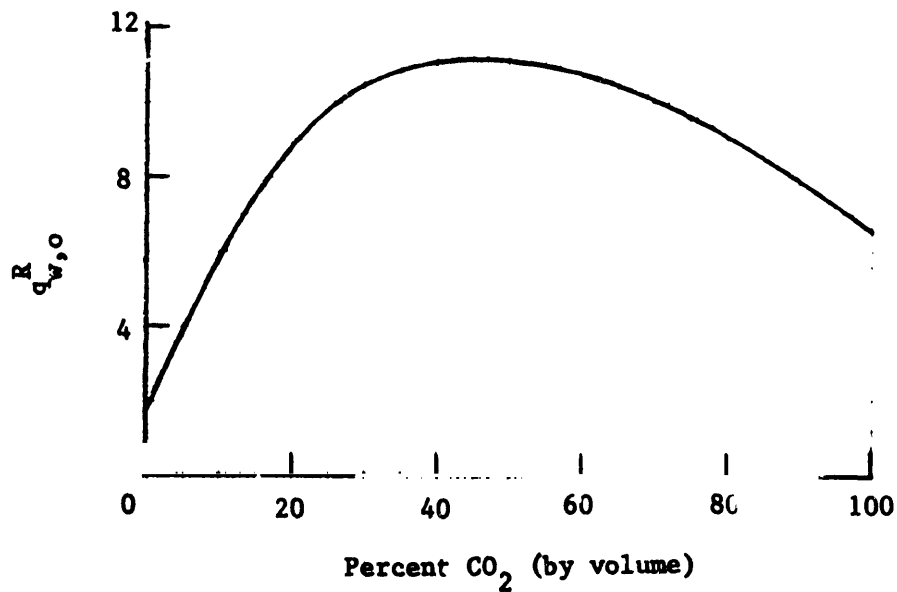WALL

s/Rn = 0
BOUNDARY-LAYER EDGE
WALL

Figure 6.- Fully coupled, radiating flow solution with steady-state ablation of carbon-phenolic heat shield for high velocity entry.
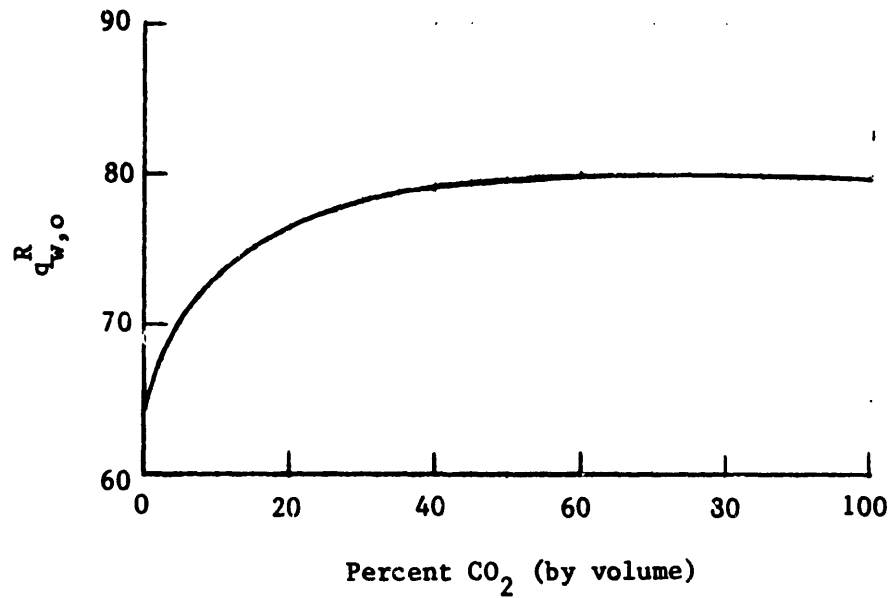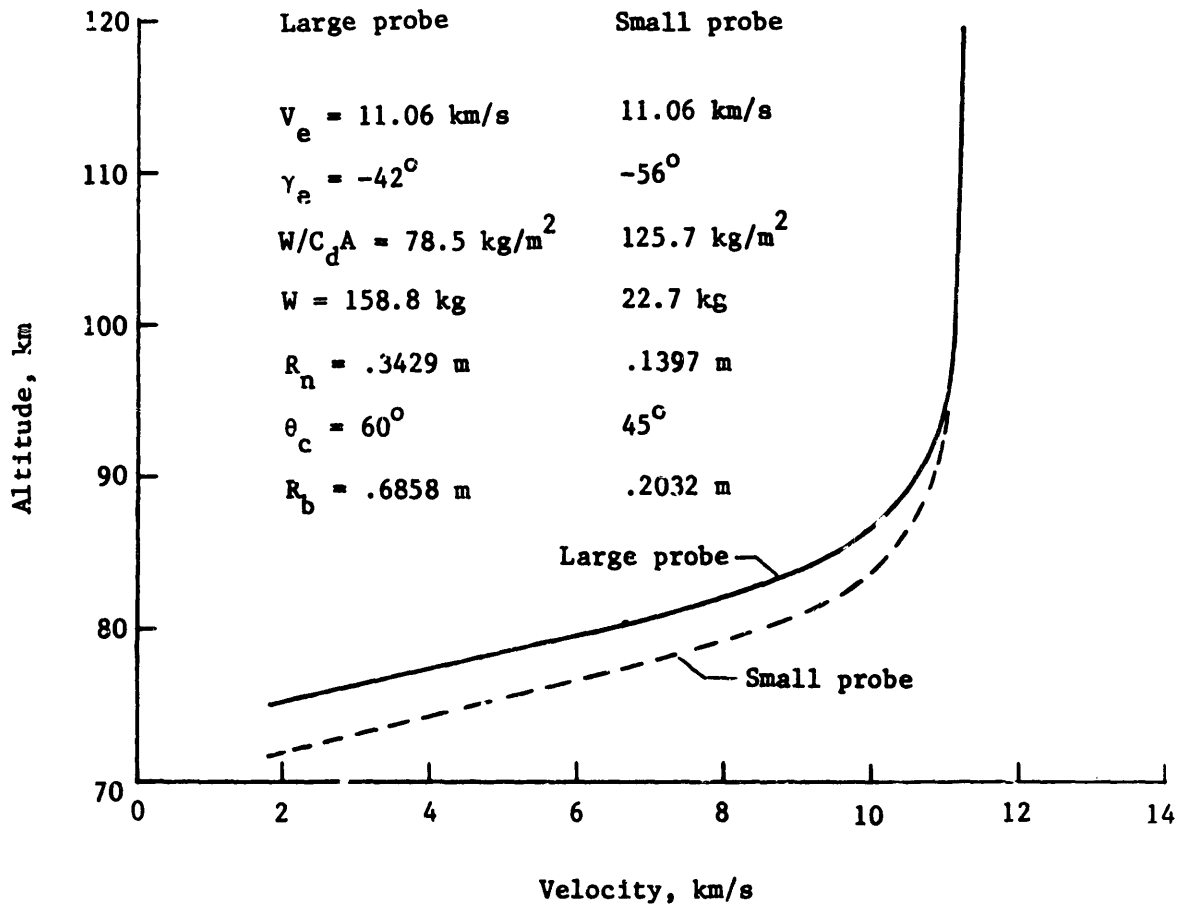
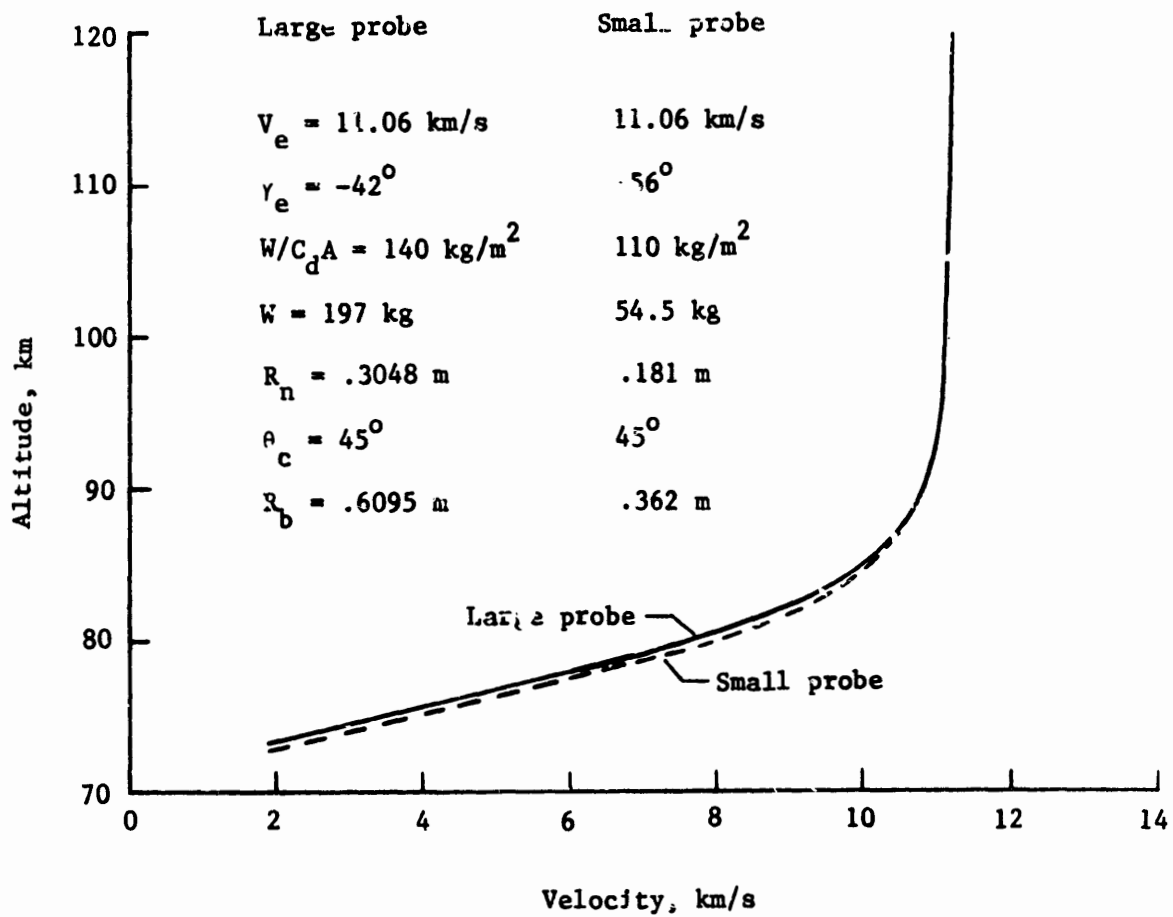(a) $V_\infty = 12.0$ km/s; $\rho_\infty = 2.99 \times 10^{-.3}$ kg/m^3.

(b) $V_\infty = 9.0$ km/s; $\rho_\infty = 5.31 \times 10^{-3}$ kg/m^3.

Figure 7.- Stagnation-point, radiative heating rates in
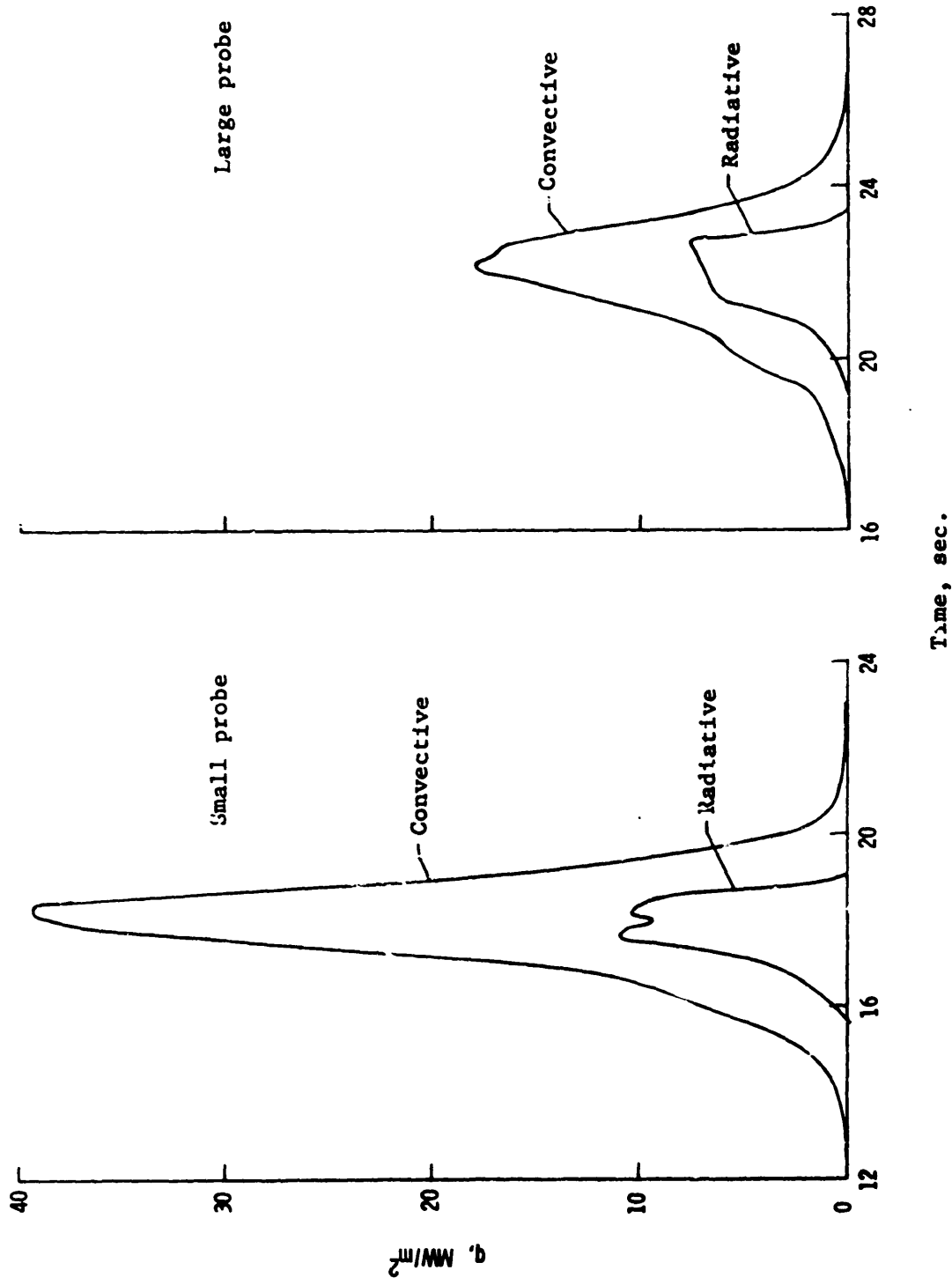CO_2-N_2 gas mixtures; $R_n = .3048$m.

(a) Type I probes

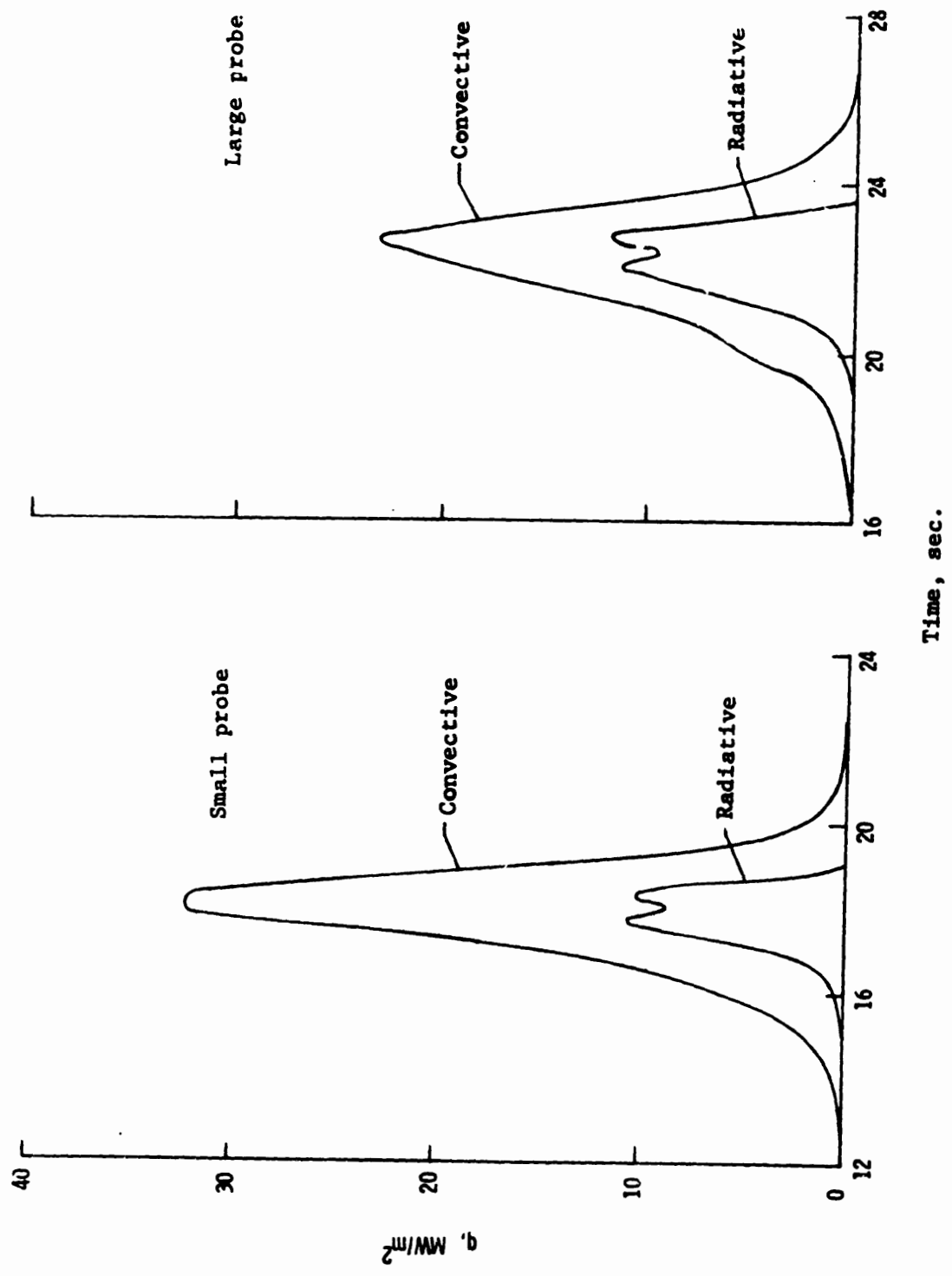Figure 8. - Trajectories for Venusian Entry.
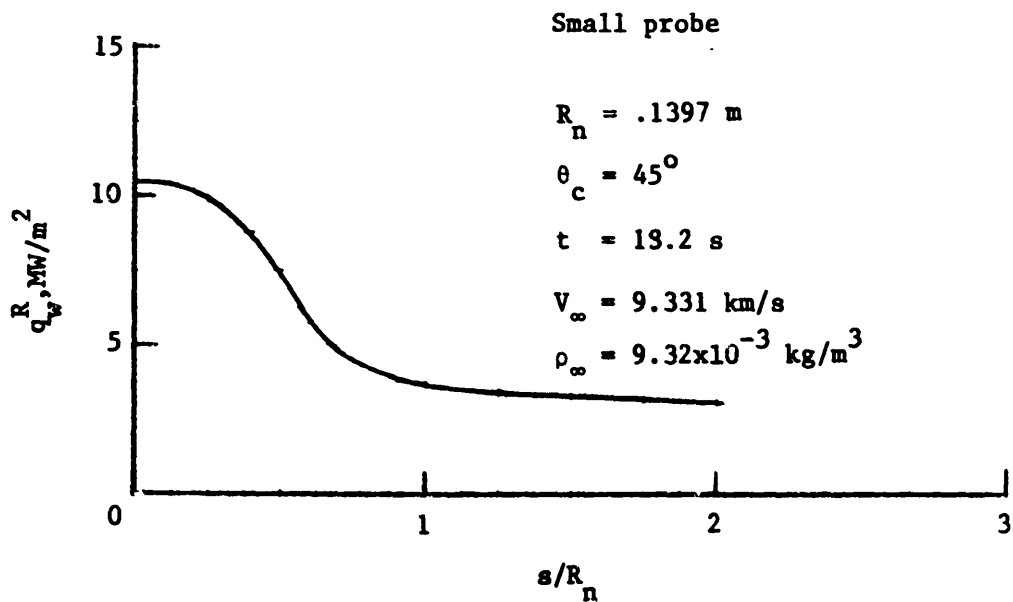
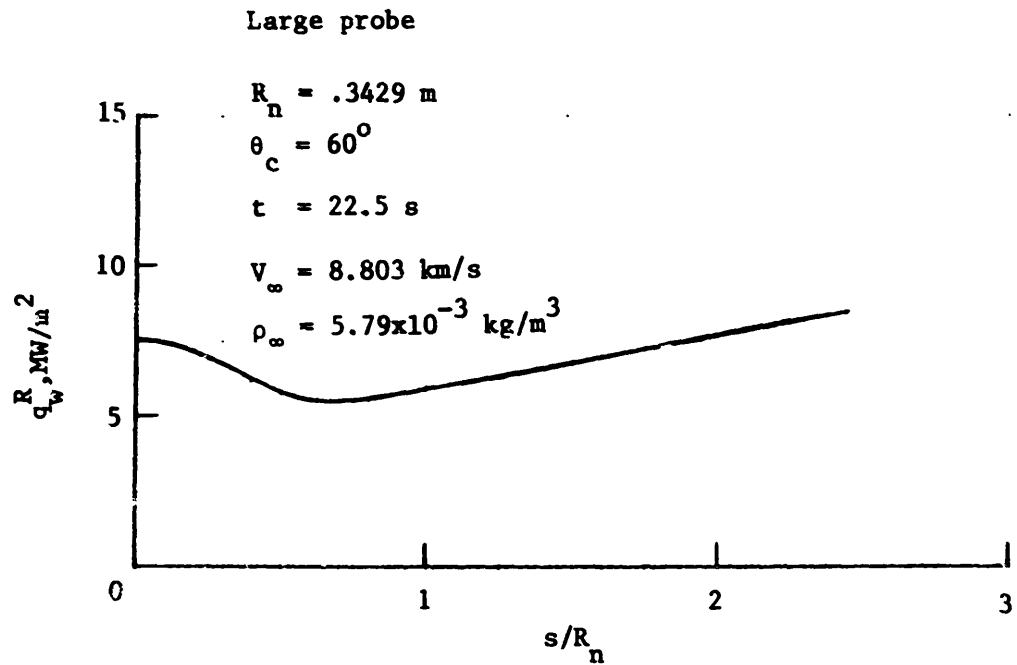(b) Type II probes

Figure 8.- Concluded.

(a) Type I probes

Figure 9.— Stagnation-point, heating rates along entry trajectories (Cold-wall, convective heating rate; Radiative heating rate from inviscid solution).
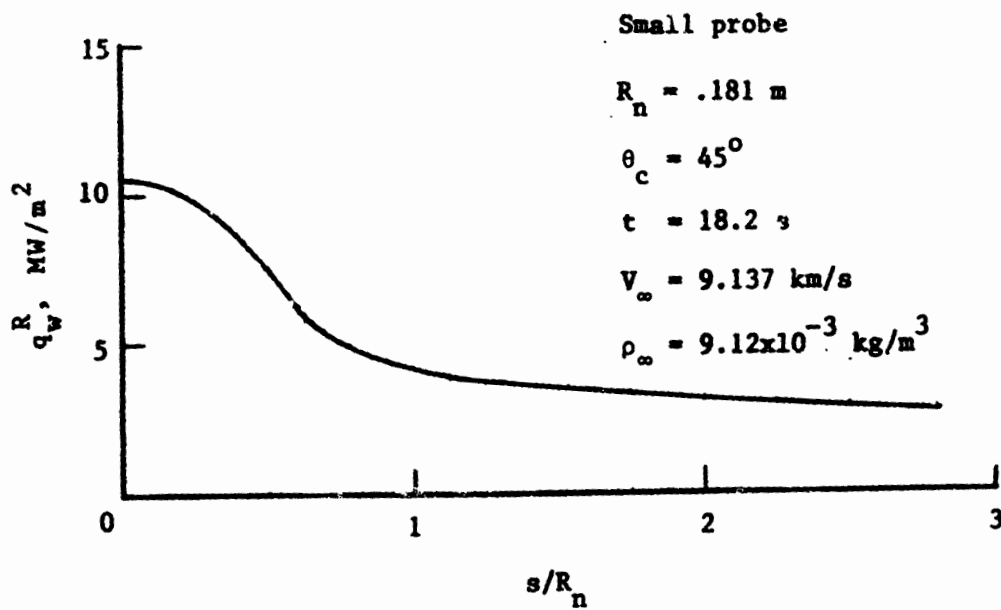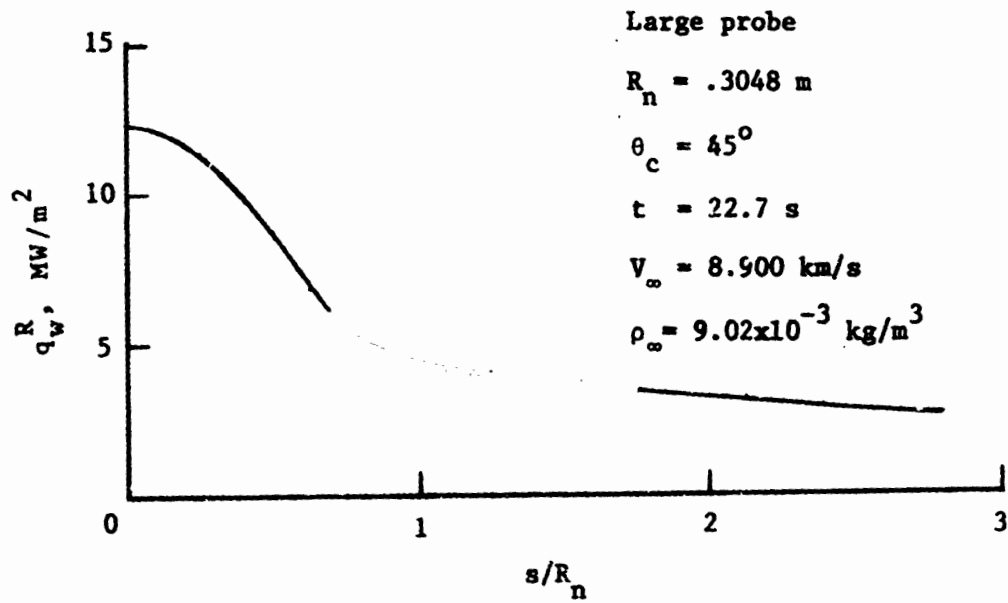
(b) Type II probes

Figure 9.- Concluded.

Large probe

$R_n = .3429$ m

$\theta_c = 60^{\circ}$

$t = 22.5$ s

$V_{\infty} = 8.803$ km/s

$\rho_{\infty} = 5.79 \times 10^{-3}$ kg/m^3

Small probe

$R_n = .1397$ m

$\theta_c = 45^{\circ}$

$t = 13.2$ s

$V_{\infty} = 9.331$ km/s

$\rho_{\infty} = 9.32 \times 10^{-3}$ kg/m^3

(a) Type I probes

Figure 10.- Radiative heating along the body at selected times on trajectories; (Radiating inviscid solution).

Large probe

R_n = .3048 m

θ_c = 45°

t = 22.7 s

V_∞ = 8.900 km/s

ρ_∞ = 9.02x10⁻³ kg/m³

Small probe

R_n = .181 m

θ_c = 45°

t = 18.2 s

V_∞ = 9.137 km/s

ρ_∞ = 9.12x10⁻³ kg/m³

(b) Type II probes

Figure 10.- Concluded.